Ninein domains required for its localization, association with partners dynein and ensconsin, and microtubule organization

Marisa M. L. Tillery[a], Chunfeng Zheng[a], Yiming Zheng[b,c], and Timothy L. Megraw[a,*]
[a]Department of Biomedical Sciences, College of Medicine, Florida State University, Tallahassee, Florida, 32306-4300; [b]State Key Laboratory of Cellular Stress Biology, School of Life Sciences, Faculty of Medicine and Life Sciences, Xiang'an Hospital of Xiamen University, Xiamen University, Xiamen, China, 361102; [c]Shenzhen Research Institute of Xiamen University, Shenzhen, China, 518057

ABSTRACT **Ninein (Nin) is a microtubule (MT) anchor at the subdistal appendages of mother centrioles and the pericentriolar material (PCM) of centrosomes that also functions to organize MTs at noncentrosomal MT-organizing centers (ncMTOCs). In humans, the *NIN* gene is mutated in Seckel syndrome, an inherited developmental disorder. Here, we dissect the protein domains involved in Nin's localization and interactions with dynein and ensconsin (ens/MAP7) and show that the association with ens cooperatively regulates MT assembly in *Drosophila* fat body cells. We define domains of Nin responsible for its localization to the ncMTOC on the fat body cell nuclear surface, localization within the nucleus, and association with Dynein light intermediate chain (Dlic) and ens, respectively. We show that Nin's association with ens synergistically regulates MT assembly. Together, these findings reveal novel features of Nin function and its regulation of a ncMTOC.**

SIGNIFICANCE STATEMENT

- Ninein is an important regulator of MTs, but its mechanism of action is mostly unknown.
- This work shows that Ninein works together with ensconsin to promote MT assembly. A predicted alpha-helical domain in Ninein associates with ensconsin and, together, Ninein and ensconsin synergistically promote MT assembly. The N-terminal domain associates with dynein light intermediate chain, consistent with human Ninein. Domains that target Ninein to the MT-organizing center and to the nucleus were also mapped.
- This work advances our understanding of Ninein's role in MT regulation through its association with ensconsin.

Monitoring Editor
Fanni Gergely
University of Cambridge

Received: Jun 26, 2023
Revised: Jun 24, 2024
Accepted: Jul 9, 2024

New Materials

This article was published online ahead of print in MBoC in Press (http://www.molbiolcell.org/cgi/doi/10.1091/mbc.E23-06-0245) on August 1, 2024.

Author contributions: MT and TM designed the study and assembled the manuscript. MT performed the experiments. CZ constructed previously-published plasmids, prepared reagents, including GFP-nanobody beads, and provided expert experimental guidance and troubleshooting. YZ performed experiments that initiated the direction of the project. All authors analyzed the data and approved the final version of the paper.

*Address correspondence to: Timothy L. Megraw (timothy.megraw@med.fsu.edu)

Abbreviations used: co-IP, co-immunoprecipitation; DCTN2-p50/Dynamitin, Dynactin 2, p50 subunit; Dhc, dynein heavy chain; Dic, dynein intermediate chain; Dlic, dynein light intermediate chain; ens, ensconsin; IF, immunofluorescence; KD, RNAi knock-down; klar, klarsicht; LamC, LaminC; LINC, linker of nucleoskeleton and cytoskeleton; MAP7, microtubule associated protein 7; Msp300, muscle-specific protein 300 kDa; msps, mini spindles; MT, microtubule; MTOC, microtubule-organizing center; ncMTOC, noncentrosomal MTOC; Nin, Ninein; Nlp, Ninein-like protein; NLS, nuclear localization signal/sequence; PCM, pericentriolar material; tub, tubulin; WB, immunoblotting/Western blot.

INTRODUCTION

Ninein (Nin) is a microtubule (MT)-anchoring protein that localizes to subdistal appendages on the mother centriole, within the pericentriolar material (PCM) at the centrosome, and at subcellular sites where noncentrosomal MT-organizing centers (ncMTOCs) are organized (Bouckson-Castaing *et al.*, 1996; Mogensen *et al.*, 2000; Dammermann and Merdes, 2002; Ou *et al.*, 2002; Delgehyr *et al.*, 2005; Dyachuk *et al.*, 2016; Kowanda *et al.*, 2016; Zheng *et al.*, 2016; Muroyama and Lechler, 2017; Sanchez and Feldman, 2017; Wu and Akhmanova, 2017; Paz and Luders, 2018; Tillery *et al.*, 2018; Vineethakumari and Luders, 2022). Mutations in *NIN*, also known as *SCKL7*, are linked to Seckel syndrome, a type of congenital microcephalic primordial dwarfism disorder (Dauber *et al.*, 2012). Underscoring its role in growth and development, Nin is essential in neural progenitor cells (NPCs) where it is needed for the asymmetric segregation of mother and daughter centrosomes (Wang *et al.*, 2009), for cell cycle-dependent nuclear movement and MT aster formation at centrosomes (Shinohara *et al.*, 2013), and for NPC maintenance and segregation behavior of the older centrosome (Royall *et al.*, 2023). During epidermal progenitor cell division, Nin is required for mitotic spindle orientation. A *Nin* null mutation is semilethal in mice, and survivors show disruption of desmosomes and lamellar body secretion in keratinocytes, resulting in a thin-skin phenotype (Lecland *et al.*, 2019). Nin mutant mice also have significant defects in bone development, with associated deficits in MT assembly from centrosomes and centrosome cohesion and clustering defects in osteoclasts (Gilbert *et al.*, 2024). In macrophages, Nin is important with dynein for phagocytosis and for phagosome trafficking (Omer *et al.*, 2024).

Ninein-like protein (Nlp), a Nin paralogue, is also a centrosomal protein (Casenghi *et al.*, 2003) with indirect links to ciliopathies (van Wijk *et al.*, 2009). Like Nin, Nlp associates with dynein (Redwine *et al.*, 2017) and γ-tubulin (Casenghi *et al.*, 2003). Nlp was shown to be an essential component of the antiviral innate immune response. *NINL* human knockout cells showed enhanced viral replication, making them more susceptible to infection (Stevens *et al.*, 2022). In contrast, *Drosophila* has just one *Nin* orthologue (also known as *Bsg25D*), and *Nin* null mutants are viable and fertile (Kowanda *et al.*, 2016; Zheng *et al.*, 2016; Rosen *et al.*, 2019). Despite these findings establishing the importance of Nin and Nlp in health and development, little is understood about the molecular functions of Nin and how it organizes an MTOC.

In addition to its localization at centrosomes, Nin is also a component of ncMTOCs where it also functions as an MT anchor (Mogensen *et al.*, 2000; Casenghi *et al.*, 2003; Delgehyr *et al.*, 2005; Wang *et al.*, 2015; Zheng *et al.*, 2016; Sanchez and Feldman, 2017; Tillery *et al.*, 2018). Examples of Nin's involvement at ncMTOCs include localizing apically in mammalian cochlear cells (Mogensen *et al.*, 2000), at the cell cortex in the murine epidermis (Lechler and Fuchs, 2007), and perinuclearly in mammalian and *Drosophila* myotubes (Bugnard *et al.*, 2005; Rosen *et al.*, 2019) and *Drosophila* larval fat body cells (Zheng *et al.*, 2020). In differentiating keratinocytes, Nin is necessary for the cortical organization of MTs and the relocalization of MT-organizing proteins to the cell cortex (Lecland *et al.*, 2019). In epithelial cells, the development of an apical-basal polar array of MTs involves a switch from centrosomal MTs that requires Nin and its trafficking by CLIP-170 (Goldspink *et al.*, 2017). In the developing vasculature, Nin is required to control tubular morphogenesis of angiogenic endothelial cells (Matsumoto *et al.*, 2008). In the mouse brain, alternative splicing of the *Nin* transcript results in expression of a noncentrosomal isoform, implicating a noncentrosomal role in neurons as well (Zhang *et al.*, 2016).

Recent findings indicate functional requirements for Nin at ncMTOCs. When centrioles are experimentally eliminated from interphase human cell culture, a single acentriolar MTOC forms from the assembly of PCM proteins CDK5RAP2, Pericentrin, Nin, and γ-tubulin. Nin is required for the assembly of this ncMTOC, acting late in the assembly process to promote a coalescence of smaller PCM clusters into a compact MTOC and for the formation of the radial MT network (Chen *et al.*, 2022).

In *Caenorhabditis elegans* larval epidermis, the *Nin* orthologue *NOCA-1* functions in parallel with the MT stabilizer and Patronin/CAMSAP orthologue *PTRN-1* to organize a ncMTOC critical for growth and morphogenesis. NOCA-1 works with γ-tubulin, while PTRN-1 does not (Wang *et al.*, 2015). In *C. elegans* neurons, dendritic ncMTOCs on RAB-11-positive vesicles require parallel activities of PTRN-1 and NOCA-2, a closer orthologue to Nin than NOCA-1 (He *et al.*, 2022).

In *Drosophila* embryonic muscle, Nin is not essential for nuclear positioning, but its loss sensitizes cells to heterozygous loss of *ens* to affect nuclear positioning. Additionally, Nin overexpression impairs nuclear positioning, but cooverexpression of *ens* suppresses this (Rosen *et al.*, 2019). In *Drosophila* larval fat body cells, a perinuclear MTOC requires the parallel activities of Nin and Patronin (Zheng *et al.*, 2020). The Nesprin Muscle-specific protein 300 kDa (Msp300) organizes the fat body perinuclear MTOC by recruiting Patronin and the MT polymerase mini spindles (msps; Zheng *et al.*, 2020). This ncMTOC controls MT assembly, nuclear positioning, and retrograde endocytic trafficking (Zheng *et al.*, 2020). The role of Nin at the fat body MTOC, however, is unclear. Although progress has been made in understanding Nin's localization to various MTOCs and its roles in cell function, development, and disease, we lack a clear understanding of how Nin functions in MT organization and MTOC control.

Human NIN binds to dynein motor (Redwine *et al.*, 2017; Celestino *et al.*, 2019; Lee *et al.*, 2020); *Drosophila* Nin binds to MTs (Kowanda *et al.*, 2016) and associates with ensconsin (ens/MAP7; Rosen *et al.*, 2019); and human, *Drosophila,* and *C. elegans* Nin orthologues all associate with γ-tubulin (Casenghi *et al.*, 2003; Delgehyr *et al.*, 2005; Lin *et al.*, 2006; Wang *et al.*, 2015; Zheng *et al.*, 2016). It is likely that these interactions are conserved across species that express Nin orthologues. Nin and Nlp associate with the dynein-dynactin complex and are activating dynein adapters (Redwine *et al.*, 2017; Reck-Peterson *et al.*, 2018; Celestino *et al.*, 2019) that bind directly to DLIC (Celestino *et al.*, 2019; Lee *et al.*, 2020). Nin transport to the centrosome is dynein-dependent as inhibiting dynein through excess p50 (Dynamitin) or p150^{glued} CC1 causes a reduction of Nin at the centrosome (Dammermann and Merdes, 2002; Casenghi *et al.*, 2005), and Nin may be trafficked along MTs via the dynein complex (Moss *et al.*, 2007). Furthermore, loss of NINL leads to a reduction in dynein-dependent transport of intracellular cargoes (Stevens *et al.*, 2022). In *Drosophila* embryonic muscle, Nin interacts and colocalizes with ens to control myonuclear positioning (Rosen *et al.*, 2019). Currently, the functional relationships between Nin and its partners are poorly understood.

To understand how Nin functions in MT assembly, we investigated the respective contributions its protein domains make to its localization at the nuclear surface and its relationships with ens and dynein. These genetic and cell biological findings indicate that multiple domains contribute to Nin localization to the nuclear surface while a central domain is responsible for localizing Nin inside the nucleus. Furthermore, we confirm that *Drosophila* Nin binds to Dlic through the N-terminus of Nin. And finally, we map the ens-binding domain to Nin and show that Nin cooperates with ens to organize MTs.

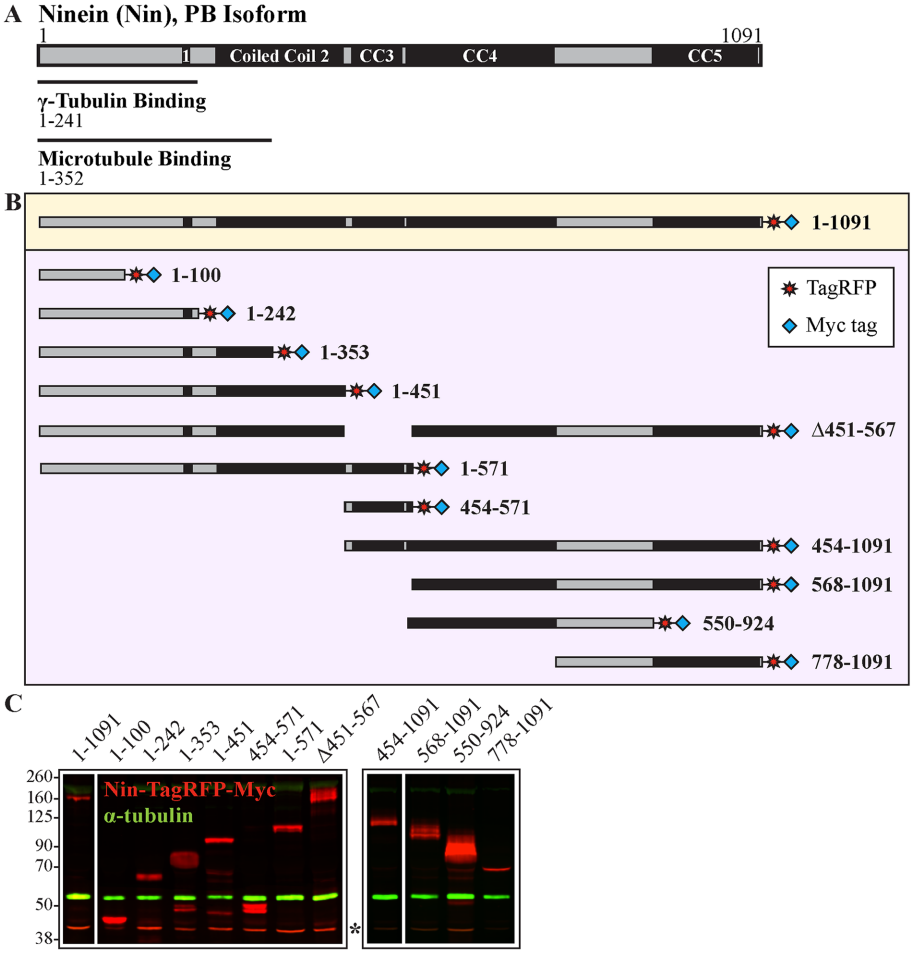

FIGURE 1: Nin transgenic constructs for in vivo structure-function analysis. (A) The full-length 1091-amino acid *Drosophila* Nin protein (isoform B), showing regions that bind γ-tubulin (aa 1-241) and MTs (aa 1-352). Solid black boxes represent predicted coiled-coil (CC) regions. (B) A full-length, transgenic construct (yellow box), in addition to 11 other constructs that divide Nin into domains (purple box) were generated for structure-function analysis. Constructs were tagged with TagRFP (red star) and Myc tags (blue diamond) at the C-terminus. Numbers reflect amino acids in Nin-PB. (C) Western blot of whole larval lysates probed with an antibody against Myc (red). Nin transgenes driven with SPARC-GAL4 express proteins of molecular weights consistent with their predicted sizes: 1-1091 = 156 kDa; 1-100 = 43.6 kDa; 1-242 = 59.2 kDa; 1-353 = 71.7 kDa; 1-451 = 83.4 kDa; 454-571 = 46.2 kDa; 1-571 = 97.1 kDa; Δ451-567 = 142.8 kDa; 454-1091 = 105.2 kDa; 568-1091 = 92.3 kDa; 550-924 = 74.1 kDa; and 778-1091 = 67.9 kDa. α-Tubulin (green, 50 kDa) served as a loading control. Asterisk denotes a nonspecific band. Black frames indicate lanes from a single gel.

RESULTS

Localization of Nin to the MTOC involves N- and C-terminal domains

We conducted a structure-function analysis of Nin (Figure 1A) in the *Drosophila* larval fat body, a tissue analogous to human liver or adipocytes that features large, monolayered cells with a perinuclear ncMTOC (Zheng *et al.*, 2020). We generated a series of transgenic constructs that express regions of Nin fused with C-terminal TagRFP and Myc tags (Figure 1, B and C). We based the design of these constructs on previously annotated domains of Nin that include the N-terminal γ-tubulin-binding (Casenghi *et al.*, 2003; Delgehyr *et al.*, 2005; Zheng *et al.*, 2016), MT-binding (Kowanda *et al.*, 2016), and dynein-binding regions of Nin (Redwine *et al.*, 2017; Celestino *et al.*, 2019) and a central region of Nin reported to bind ens (Rosen *et al.*, 2019).

Taking advantage of the *Drosophila* UAS-GAL4 binary expression system, we individually expressed these transgenes using SPARC-GAL4, a fat body driver, to evaluate their subcellular localizations in fat body cells (Figure 2; Supplemental Figure 1A). Co-IP of full-length Nin (Nin$^{1\text{-}1091}$-TagRFP-Myc) with Nin-GFP indicated that Nin can multimerize (Supplemental Figure 1B), so we compared Nin localization in a *Nin^{1}* null mutant background (Figure 2) to a wild-type background (Supplemental Figure 1A). Localization patterns, however, did not differ whether endogenous Nin was absent (Figure 2) or present (Supplemental Figure 1A).

Nin$^{1\text{-}1091}$ localized to the nuclear surface in fat body cells (Figure 2; Supplemental Figure 1A). Localization was most prominent at the nuclear surface with a weaker signal present inside the nucleus (Figure 2). Perinuclear localization in punctate aggregates was variably present, which appeared to be due to overexpression as it was more prominent with two copies of the transgene than with one (Supplemental Figure 2A). Intranuclear localization also increased with two copies of Nin$^{1\text{-}1091}$ (Supplemental Figure 2A). Expression of two Nin transgenes that express at higher levels, Eos-Nin and Nin-GFP (Supplemental Figure 2B), resulted in large intranuclear and cytoplasmic punctate aggregates (Supplemental Figure 2C), indicating that these intranuclear and aggregate patterns correlate with a high dosage effect of Nin overexpression.

High levels of ubiquitous Nin overexpression are lethal ([Zheng *et al.*, 2016] and Supplemental Figure 2D) and toxic in the fat body and muscle (Supplemental Figure 2D). Levels of Nin$^{1\text{-}1091}$ overexpression used in this study were not lethal in the fat body or muscle. However, ubiquitous overexpression of one copy of Nin$^{1\text{-}1091}$ with tub-GAL4 was semilethal (Supplemental Figure 2D), and its overexpression in the fat body with SPARC-GAL4 was not lethal but increased nuclear mispositioning (Supplemental Figure 3A). Overexpression with SPARC-GAL4 of two copies of Nin$^{1\text{-}1091}$ or other Nin transgenes that express at higher levels was lethal (Supplemental Figure 2B). Overexpression of each of the Nin transgenes shown in Figure 1 was not lethal in the fat body using SPARC-GAL4 (unpublished data).

Expression of Nin-TagRFP-Myc constructs containing N- (Nin$^{1\text{-}353}$ and Nin$^{1\text{-}451}$) or C-terminal (Nin$^{568\text{-}1091}$, Nin$^{550\text{-}924}$, and Nin$^{\Delta 451\text{-}567}$) domains localized predominantly to the nuclear surface (Figure 2; Supplemental Figure 1). An N-terminal fragment, Nin$^{1\text{-}100}$, localized mostly inside the nucleus (Figure 2; Supplemental Figure 1) and was the only construct to affect nuclear morphology by increasing nuclear circularity in the *Nin^{1}* background, albeit to a small degree (Supplemental Figure 3B). Interestingly, a central region of Nin (Nin$^{454\text{-}571}$) also localized intranuclearly but, unlike the N-terminal 100 amino acids, drove all fragments containing it

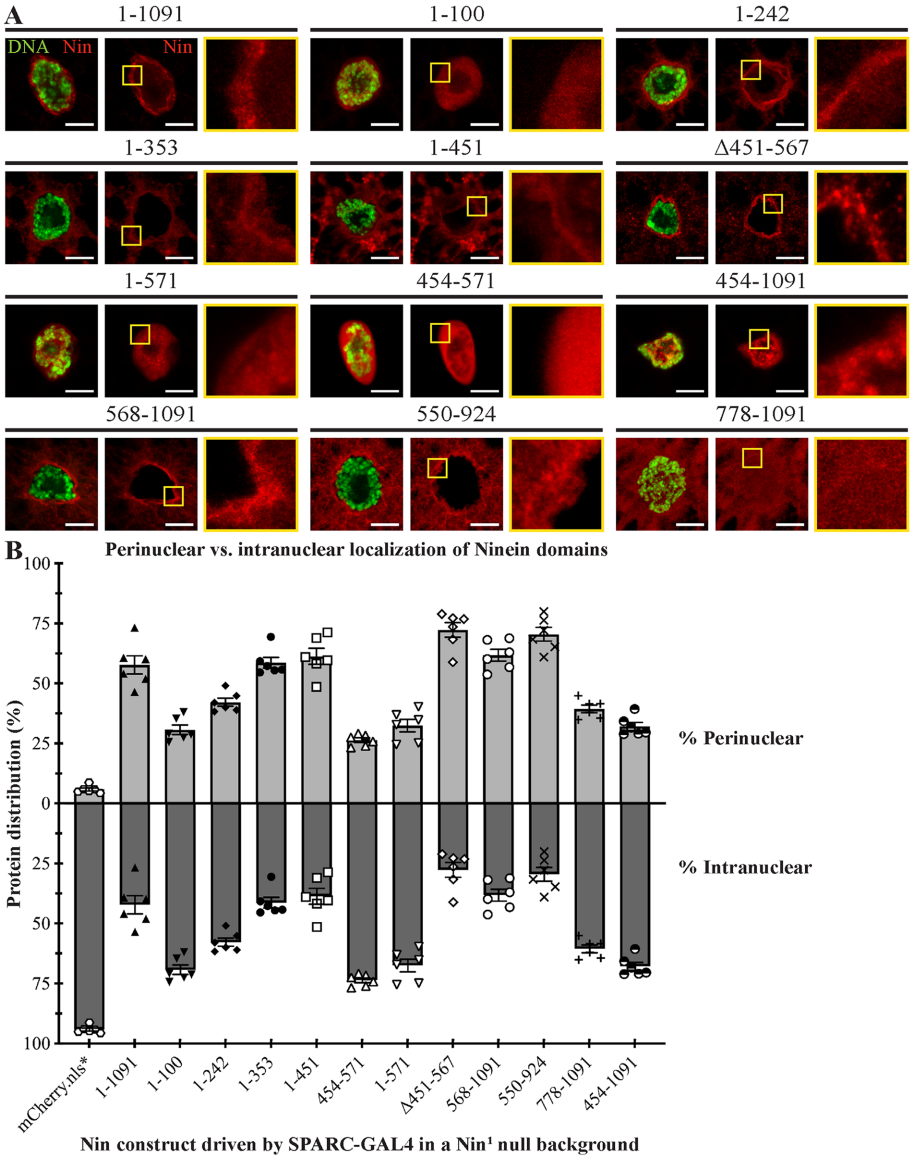

FIGURE 2: Multiple Nin domains localize to the nuclear surface or inside the nucleus. IF staining of DNA (DAPI, green) in *Nin*^{1} null mutant larval fat body cells expressing Nin transgenic constructs (TagRFP fluorescence, red). Scale bar = 10 μm in this and all subsequent figures. (A) Localization patterns of TagRFP-Myc-labeled Nin transgenes expressed in *Nin*^{1} null mutant fat body cells. Boxed yellow regions are a magnified view of the nuclear surface. Multiple domains of Nin localize to the MTOC. Nin$^{1\text{-}100}$ and fragments containing amino acids 454–567 localize predominantly intranuclearly. (B) Quantification of results in (A). Six larvae from three experiments involving ~100 cells per construct were measured for the relative localization of Nin at the periphery or inside the nucleus. Bars indicate the relative (percent) localization of Nin to the perinuclear surface versus inside the nucleus.

into the nucleus (Figure 2; Supplemental Figure 1). We used two programs to identify a potential nuclear localization signal (NLS) in these regions (see *Materials and Methods*), but none were predicted. While amino acids 454–567 target all fragments that contain it into the nucleus, this region is less efficient at targeting the full-length protein in the nucleus, possibly due to the presence of competing domains that localize Nin to the nuclear surface. Large fragments that lack this domain, including Nin$^{\Delta 451\text{-}567}$, were primarily perinuclear (Figure 2; Supplemental Figure 1). These data indicate that at least two domains of Nin contribute to its localization to the nuclear surface while amino acids 454–567 drive the protein into the nucleus and Nin1-100 can passively localize there.

MT-dependent and -independent modes of Nin localization to the MTOC

Because Nin binds MTs and is an MT anchor (Mogensen *et al.*, 2000; Abal *et al.*, 2002; Delgehyr *et al.*, 2005; Kowanda *et al.*, 2016), we next sought to determine whether MTs play a role in Nin localization at the nuclear surface. Overexpression of Nin-TagRFP-Myc constructs variably affected MT organization in null or wild-type backgrounds with varied significance (Supplemental Figure 3C). However, disrupting MTs by overexpressing the MT-severing enzyme *spastin* or by knocking down the MT component *α-tubulin* by RNAi reduced, but did not eliminate, perinuclear localization of Nin$^{1\text{-}1091}$ while increasing the incidence of punctae formation (Figure 3). Thus, there appears to be MT-dependent and -independent modes of Nin localization to the nuclear surface.

We next sought to determine which proteins anchor or recruit Nin to the nuclear surface. Our previous work showed that the Linker of Nucleoskeleton and Cytoskeleton (LINC) complex protein Msp300/Nesprin was a major structural component of the fat body MTOC required to recruit msps and Patronin to the nuclear surface to organize and assemble MTs there (Zheng *et al.*, 2020). Knockdown of *Msp300* in the fat body increased nuclear mispositioning due to MT disruption (Zheng *et al.*, 2020). Loss of *Msp300* (Figure 4A) or *Patronin* (Figure 4B) reduced perinuclear Nin and increased its intranuclear localization and cytoplasmic aggregate accumulation (Figure 4, A and B, arrowheads). However, there was no overt effect on localization of Nin to the nuclear surface when *msps* (Figure 4C) or the other *Drosophila* Nesprin *klarsicht* (*klar*) was knocked down (Figure 4D). Therefore, Nin localization to the nuclear surface relies partly on MTs, but also on a MT-independent anchor that involves Msp300 and Patronin. Whether these interactions are direct or indirect remains to be determined.

Ensconsin but not dynein is required for Nin localization to the MTOC

We next analyzed whether Nin requires dynein and/or ens for localization. Loss of *Dynein heavy chain* (*Dhc*) or *Dynein light intermediate chain* (*Dlic*), a direct partner of NIN (Celestino *et al.*, 2019; Lee *et al.*, 2020), blocks the trafficking of Rab5 vesicles from the cell membrane to the nuclear periphery ((Zheng *et al.*, 2020) and Supplemental Figure 4A). Furthermore, depletion of dynein subunits or dynein inactivation from the overexpression of *DCTN2-p50/Dynamitin* did not alter MT organization (Zheng *et al.*, 2020), nor did it visibly reduce perinuclear Nin localization

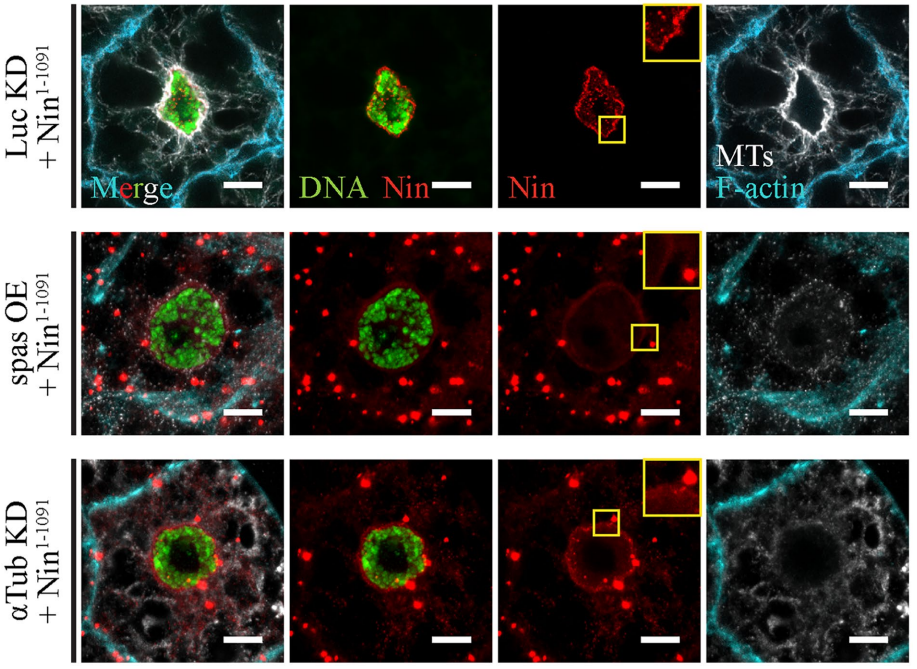

FIGURE 3: Localization of Nin to the fat body ncMTOC is partially dependent upon MTs. IF staining of larval fat body cells with DNA (DAPI, green), Nin$^{1-1091}$ (TagRFP fluorescence, red), F-actin (488 Phalloidin, cyan), and MTs (YL1/2, white). Insets show an enlarged view of the nuclear surface. Nin$^{1-1091}$ localizes to the perinuclear MTOC and forms aggregates when MTs are disrupted by the overexpression (OE) of *CFP-spastin* or by the RNAi-mediated KD of *α-tubulin*. Experiment was repeated at least nine times and included >18 larvae.

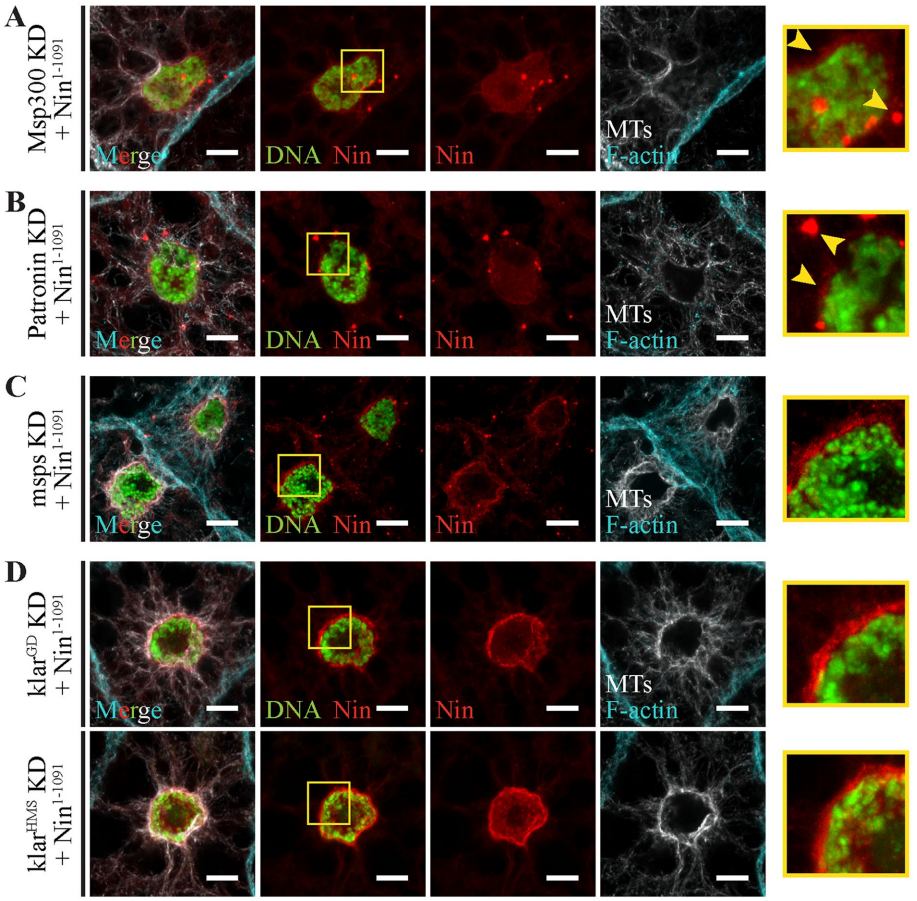

(Figure 5A). Loss of *ens*, on the other hand, did disrupt Nin localization to the nuclear surface, resulting in perinuclear Nin aggregate formation (Figure 5B).

Nin interacts with ens and Dlic

We next aimed to determine how Nin coordinates MT organization and if its partners play a role by first confirming whether Nin associates with ens and/or dynein in fat body cells. We overexpressed Nin-GFP in fat body cells using SPARC-GAL4, treated lysates with nocodazole on ice to depolymerize MTs, and pulled down Nin-GFP using GFP nanobody beads. We detected an association with endogenous ens (Figure 6A). Using the Nin constructs (Figure 1), we further mapped the interaction domain by overexpressing ens-GFP together with various Nin constructs in fat bodies, pulling down ens-GFP, and probing for the Myc tag on Nin fragments. The C-terminus of Nin (Nin$^{568-1091}$ and Nin$^{550-924}$) coimmunoprecipitated with ens (Figure 6B, green arrows), but a large N-terminal portion (Nin$^{1-571}$) and a C-terminal portion (Nin$^{778-1091}$) did not (Figure 6B, red arrows). We infer from the co-IP data that the minimum interaction domain between Nin and ens is within amino acids 568–777 of Nin (Figure 6B, see also Figure 7).

Using a similar approach, we mapped the domain that binds dynein. In agreement with previous work that identified NIN as an activator of dynein (Redwine *et al.*, 2017; Reck-Peterson *et al.*, 2018) that binds directly to DLIC1 and DLIC2 via its N-terminal 87 amino acid EF hand domains (Celestino *et al.*, 2019; Lee *et al.*, 2020), the N-terminus of *Drosophila* Nin (Nin$^{1-100}$ and Nin$^{1-451}$) coimmunoprecipitated with Dlic-GFP (Figure 6C, green arrows) while central (Nin$^{454-571}$)

FIGURE 4: Fat body MTOC proteins Msp300 and Patronin are necessary for perinuclear Nin localization. IF staining of larval fat body cells expressing Nin$^{1-1091}$ using SPARC-GAL4 in a wild-type background with RNAi KD of the genes indicated. DNA (DAPI, green), Nin$^{1-1091}$ (TagRFP fluorescence, red), F-actin (488 Phalloidin, cyan), and MTs (YL1/2, white). The right panels show an enlarged view of the nuclear surface. Experiments were repeated at least nine times and included >18 larvae. (A and B) KD of *Msp300* or *Patronin* reduces Nin localization to the nuclear surface and increases the formation of cytoplasmic aggregates (arrowheads). (C and D) KD of *msps* or *klar* using either of two RNAi lines (GD9271 above, HMS01612 below) does not affect Nin localization.

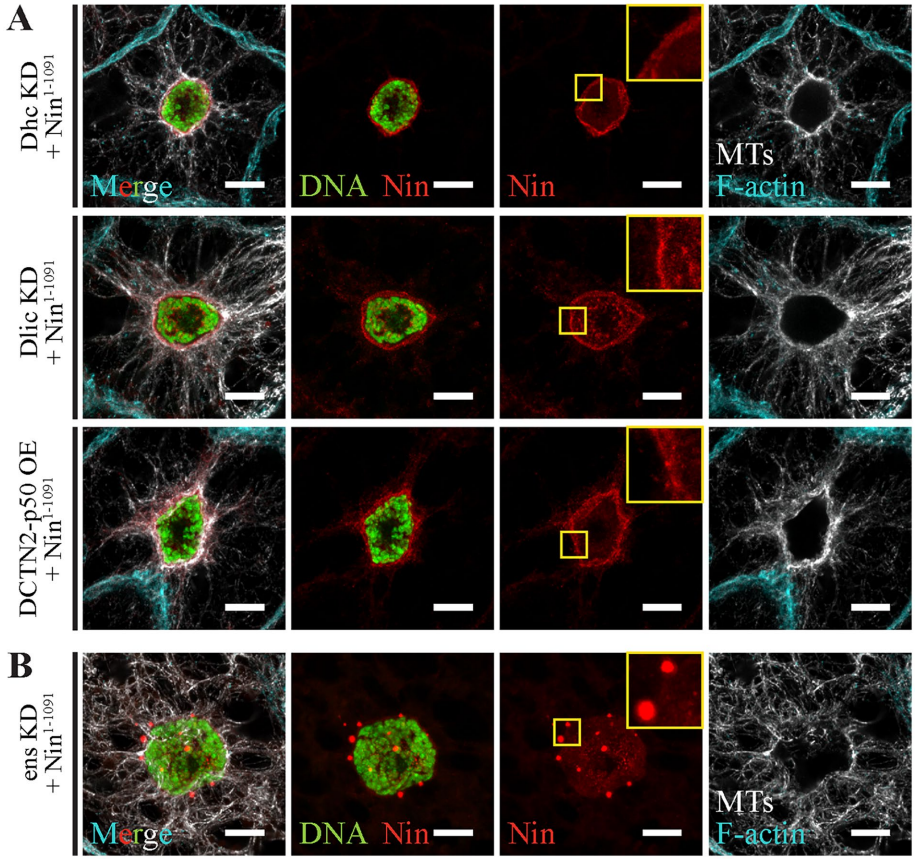

FIGURE 5: Nin localization is dependent upon ensconsin, not dynein. IF staining of larval fat body cells expressing Nin^{1-1091} using SPARC-GAL4 in a wild-type background with RNAi KD of the genes indicated. DNA (DAPI, green), Nin^{1-1091} (TagRFP fluorescence, red), F-actin (488 Phalloidin, cyan), and MTs (YL1/2, white). Insets show an enlarged view of the nuclear surface. Experiments were repeated at least 6 times and included >12 larvae. (A) KD of *Dynein heavy chain* (*Dhc*) or *Dlic* or inactivation of the dynein motor with *DCTN2-p50/Dynamitin* overexpression (OE) does not affect Nin localization to the MTOC. (B) Loss of *ensconsin* (*ens*) perturbs Nin localization, causing it to aggregate near the nucleus.

and C-terminal Nin fragments ($Nin^{454-1091}$ and $Nin^{568-1091}$) did not (Figure 6C, red arrows). A longer N-terminal fragment, Nin^{1-571}, was unexpectedly not detected in the co-IP with Dlic-GFP, possibly due to lower expression levels. We were unable to detect an association between Dynein intermediate chain (Dic) and Nin (Supplemental Figure 4B). A summary of the mapping of ens and Dlic binding domains to Nin is shown in Figure 8.

Nin synergizes with ens to promote MT assembly

Our next goal was to evaluate whether Nin's interaction with dynein or ens was sufficient for MTOC formation. Ens and Dlic colocalize with MTs at the MTOC (Supplemental Figure 5, A and B). Dlic-GFP was predominantly nuclear when overexpressed and appeared to drive full-length Nin into the nucleus (Supplemental Figure 5C). Remarkably, cooverexpression of ens-GFP with full-length Nin or constructs containing a region near Nin's C-terminus ($Nin^{454-1091}$, $Nin^{568-1091}$, and $Nin^{550-924}$) produced robust juxtanuclear MTOCs that superseded the perinuclear MTOC (Figure 7A). Overexpression of Nin or ens alone did not induce an ectopic MTOC, whereas together, they synergize to organize MTs. These robust, ectopic MTOCs disrupted nuclear integrity as evidenced by alterations to the pattern of LaminC (LamC), a nuclear lamin nucleoskeleton component (Figure 7B, orange arrowheads). LamC staining was diminished at the nucleus adjacent to the position of the ectopic MTOC (Figure 7B, orange arrowheads), and chromosomal material appears to have spilt into the cytoplasm (Figure 7B, yellow arrowheads).

We infer from these results that amino acids 568-777 of Nin are sufficient for the formation of an MTOC in cooperation with ens. This is consistent and overlaps with the MT-independent ens-interacting domain identified from the co-IP experiments (see Figure 6B). When MTs are disrupted, Nin and ens still coalesce, but fail to organize into a single focus, indicating that MTs contribute to the organization of the single ectopic MTOC (Supplemental Figure 5D). The synergy between Nin and ens in forming an MTOC is unique to that partnership as overexpression of Nin^{1-1091} together with either Dlic or Dhc did not overtly alter MT organization (Supplemental Figure 5C).

DISCUSSION

In this study, we generated a set of transgenic Nin deletion constructs in *Drosophila* that enabled us to map Nin's localization, partner-binding, and MT-regulating domains in vivo in the larval fat body. From these data, we identify domains of Nin that contribute to its localization at the MTOC on the nuclear surface and inside the nucleus, we confirm the orthologous association of the N-terminus with Dlic that was previously mapped on human Nin, and we map the domain that associates with ens (Figure 8). From coexpression assays, we found a synergistic interaction between ens and Nin's ens-binding domain that is sufficient to generate a robust ectopic MTOC.

Full-length tagged Nin (Nin^{1-1091}) localizes primarily to the nuclear surface, while lower levels are detected inside the nucleus. We further determined that a 114-amino acid domain at positions 454–567 is necessary and sufficient to target Nin into the nucleus (Figure 8, A and B, green). All subfragments of Nin containing this domain showed significant localization within the nucleus; however, the full-length Nin protein had relatively low levels inside the nucleus, possibly due to the presence of competing domains in the N- and C-terminal regions that target Nin to the nuclear surface. A construct lacking this domain ($Nin^{\Delta 451-567}$) localized less within the nucleus than full-length Nin, reinforcing the significance of this domain in targeting Nin to the nucleus.

Localization of Nin to the nucleus was shown in human cultured cells overexpressing hNinein (Cheng *et al.*, 2006) and in *Drosophila* muscle cells overexpressing *Drosophila* Nin (Rosen *et al.*, 2019). In both cases, nuclear localization was linked to Nin SUMOylation (Cheng *et al.*, 2006; Rosen *et al.*, 2019). If this mechanism holds in fat body cells, it suggests that the nuclear targeting domain identified at 454-567 in *Drosophila* Nin is a candidate domain for SUMO modification.

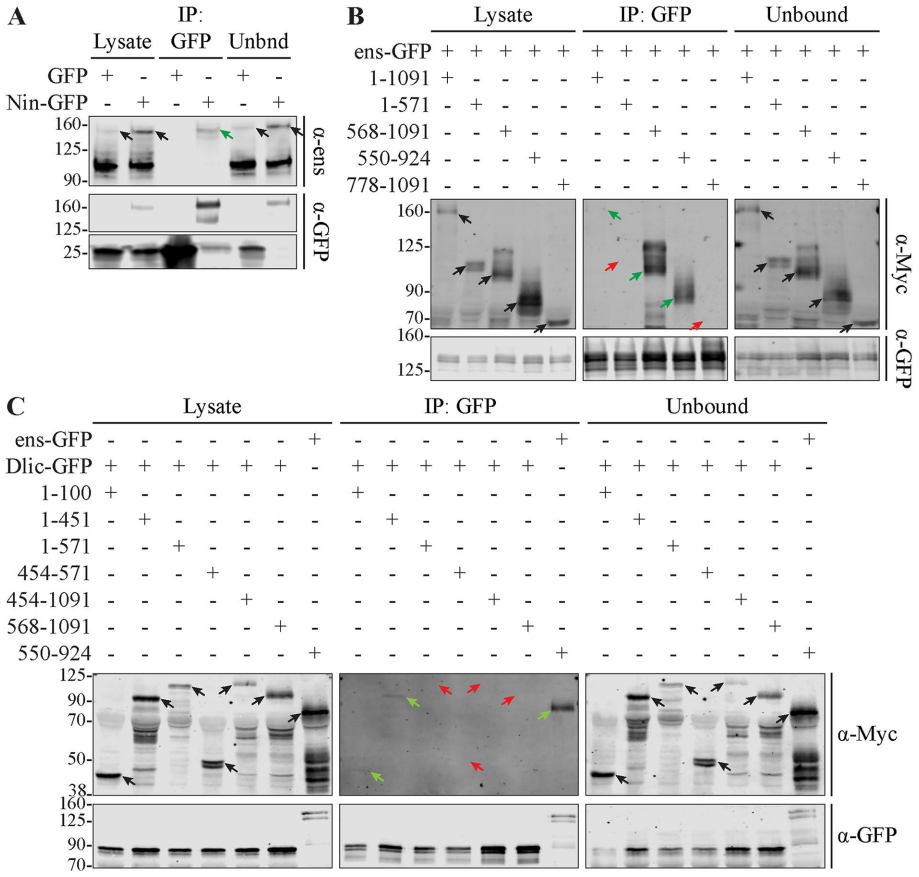

FIGURE 6: Mapping of Nin's ens- and Dlic-interaction domains. Western blot analysis of GFP immunoprecipitates from whole larval lysates expressing the indicated proteins in fat bodies. Unbnd = Unbound fraction in lysate after IP. Green arrows indicate a positive co-IP, and red arrows, a negative. co-IPs were repeated at least three times. (A) co-IP of ens with Nin-GFP. The membrane was probed for endogenous ens (~150 and 100 kDa) and GFP. Endogenous ens (~150 kDa) coimmunoprecipitated with Nin. (B) co-IP of Nin-TagRFP-Myc fragments with ens-GFP. The membrane was probed for GFP (ens-GFP; ~180 kDa) and Myc (Nin; various sizes). (C) co-IP of Nin-TagRFP-Myc fragments with Dlic-GFP. The membrane was probed for GFP (Dlic-GFP; ~81 kDa) and Myc (Nin; various sizes). $Nin^{550\text{-}924}$ + ens-GFP was used as a positive control.

Expression of the N-terminal 100 amino acids of Nin was also localized within the nucleus, but larger fragments that included this domain did not localize predominantly within the nucleus. Therefore, unlike the nuclear localization domain at 454-567, this domain was not sufficient for targeting, and we suggest that it passively localizes into the nucleus due to its small size and may not play a role in the nuclear localization of full-length Nin. The expected molecular weight of this domain with the engineered tag is ~44 kDa, which is within the limits (30–60 kDa) of passive diffusion between nucleus and cytoplasm (Keminer and Peters, 1999; Wang and Brattain, 2007; Timney *et al.*, 2016). This could explain why longer fragments such as $Nin^{1\text{-}353}$ and $Nin^{1\text{-}451}$ do not prominently localize inside the nucleus but are instead localized primarily to the perinuclear MTOC.

N- and C-terminal Nin-TagRFP-Myc constructs localize to the MTOC at the nuclear surface. The contribution of multiple domains of Nin conferring localization to the MTOC may point to its interactions with several distinct partners, including MTs, ens, etc. that anchor Nin at the MTOC. The fat body nuclear surface has prominent circumferential MTs (Zheng *et al.*, 2020), and recruitment of full-length Nin is largely, but not completely, dependent on them. Depolymerizing MTs may release a MT-interacting pool of Nin, freeing up Nin to aggregate, a phenotype similar to higher levels of Nin overexpression. We propose that Nin localizes to the nuclear surface through a combination of MT-dependent and -independent modes, with the MT-independent mode being dependent on Msp300, Patronin, and/or ens. Nin is a MT-associated protein, and so the MT-dependent mode is likely attributed to the high density of circumferential MTs associated with the fat body nucleus. Both pools of Nin likely contribute to MTOC function.

Human DLIC1 was shown to bind directly to NIN via a pair of Ca^{++}-independent EF hand domains at the N-terminal 87 amino acids of NIN (Lee *et al.*, 2020), a region that is highly conserved between human and *Drosophila* nineins (Zheng *et al.*, 2016). We confirm that *Drosophila* Nin is also associated with Dlic and have mapped this interaction to the N-terminal end of Nin (Figure 8, A and B, pink).

When Dlic-GFP was overexpressed in fat body cells, it localized in the nucleus. This was unexpected as Dlic's role as a subunit of the dynein motor complex places its function with MTs in the cytoplasm. Other studies have used this and other tagged UAS-Dlic transgenes in tissues other than the fat body; however, their localization was not detected or reported to be nuclear (Pandey *et al.*, 2007; Emre *et al.*, 2011; Wainman *et al.*, 2012; Baumbach *et al.*, 2015; Inaba *et al.*, 2015). Endogenous Dlic localized at the plasma membrane and at the perinuclear MTOC. Although Dlic-GFP overexpression drove Nin into the nucleus, this nuclear localization dynamic did not overtly impact MT organization. Furthermore, loss of either Dhc or Dlic or inactivation of dynactin does not affect Nin localization to the perinuclear MTOC or MT organization in fat body cells. Although the interaction between Nin and Dlic may be important in other cellular processes, this study did not reveal a role for it in MT organization in the fat body.

From the co-IP data, we identified a Nin-ens interaction domain between amino acids 568–777 of Nin (Figure 8, A and B, yellow), which was consistent with the colocalization of Nin and ens from IF staining. We further demonstrated that, when overexpressed, Nin and ens function synergistically to form an ectopic ncMTOC. When Nin constructs that include amino acids 568–777 are overexpressed with ens, robust ectopic MTOCs are formed adjacent to the nucleus. Interestingly, Nin's interaction with overexpressed ens is sufficient to overcome Nin's nuclear localization (compare $Nin^{454\text{-}1091}$ Figure 7, A and B to Supplemental Figure 1A). In contrast to the developing muscle, where

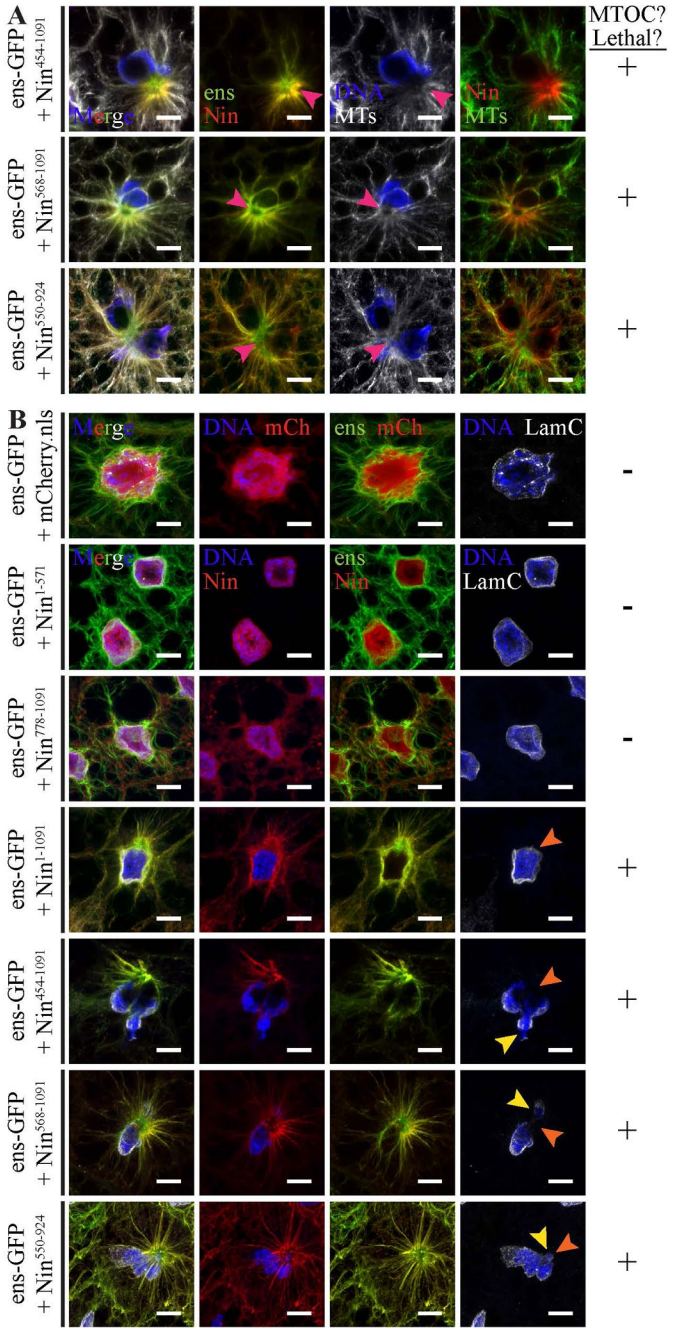

FIGURE 7: Nin and ensconsin synergize to form an ectopic MTOC that disrupts nuclear morphology. DNA (DAPI, blue), Nin$^{1\text{-}1091}$ (TagRFP fluorescence, red), ens (GFP fluorescence, green), and MTs (YL1/2, white) or LamC (LC28.26, white). (A) Cooverexpression of ens and fragments that include amino acids 568–777 of Nin alters MT organization, forming a robust juxtanuclear MTOC (pink arrowheads) associated with late pupal lethality. (B) LamC staining labels the inner nuclear membrane and is reduced where Nin-ens ectopic MTOCs are formed (orange arrowheads). Additionally, nuclear DNA spills into the cytoplasm (yellow arrowheads).

multiple foci formed from Nin-ens overexpression (Rosen *et al.*, 2019), there is only one Nin-ens MTOC per fat body cell. Overexpression of Nin-TagRFP-Myc fragments or ens-GFP alone in the fat body produced no overt effects, and flies were viable, whereas cooverexpression of fragments containing Nin's ens-binding domain together with ens-GFP was late pupal lethal. In contrast with these synergistic effects of Nin and ens expression in the fat body, similar overexpression experiments in the developing muscle showed that Nin overexpression was lethal and was suppressed, rather than enhanced, by cooverexpression of ens (Rosen *et al.*, 2019). Higher expression of Nin in the fat body above the levels achieved with Nin-TagRFP-Myc (expression of 2X Nin-TagRFP-Myc, Nin-GFP, or Eos-Nin) was lethal, but the cause of lethality is unclear. Whether the MTOC that Nin-ens generates involves other factors remains to be determined. It likely does not require γ-tubulin because γ-tubulin is expressed at very low levels in the fat body and was not required for MT assembly at the primary fat body MTOC (Zheng *et al.*, 2020).

In the fat body, Nin-ens ectopic MTOCs were positioned near the nucleus, disrupted the nuclear envelope, altered nuclear morphology, and resulted in the leakage of chromosomal material into the cytoplasm. One function of the fat body MTOC under normal conditions may be to ensure proper nuclear morphology. Normally, MTs in the fat body are organized both in circumferential bundles surrounding and with their minus ends anchored at the nuclear surface (Zheng *et al.*, 2020). With the generation of Nin-ens ectopic MTOCs, the nuclear morphology changes appear to be the result of the forces generated by imposing MTs emanating from the newly established ectopic MTOC as depletion of MTs under these conditions attenuated disruption of nuclear morphology. The disruption of LamC patterning at the nuclear periphery is consistent with the fragility of these nuclei, as mutations in lamins can produce a similar phenotype (Davidson and Lammerding, 2014). Moreover, impinging MTs can impact nuclear morphology, a phenomenon also correlated with the reduction of lamin signal (Biedzinski *et al.*, 2020; Heffler *et al.*, 2020). LamC signal was not disrupted by Nin-ens cooverexpression when MTs were also disrupted, pointing to the role of Nin-ens-organized MTs in nuclear morphology changes and the loss of structural integrity of the nucleus. Presumably, the lethality associated with Nin and ens cooverexpression is due to these nuclear disruptions.

Altogether, our findings reveal novel features of domains required for Nin's localization to the fat body MTOC on the nuclear surface, localization inside the nucleus, its interactions with dynein and ens, and how those interactions impact Nin localization and MT organization in fat body cells. Furthermore, we identify a synergistic effect between Nin and ens capable of coordinating an MTOC, implying a mechanistic connection between this partnership normally at the fat body perinuclear and possibly at other MTOCs. It will be interesting to discover whether human NIN has a cooperative role with MAP7 (ens orthologue) in organizing MTs and whether this connection has disease relevance.

MATERIALS AND METHODS

Request a protocol through *Bio-protocol*.

Generation of UAS-Nin-TagRFP-Myc transgenes

The Nin coding sequence (*Nin-RB* isoform) was amplified by polymerase chain reaction (PCR) from the LD21844 cDNA clone (RRID:DGRC_5314) using the primers 1.FWD and 1.REV. The PCR product, which included the entire ORF, was cloned into the pENTR/D-TOPO vector (Thermo Fisher Scientific, Catalogue #K240020). Using Gateway LR cloning, the coding sequence

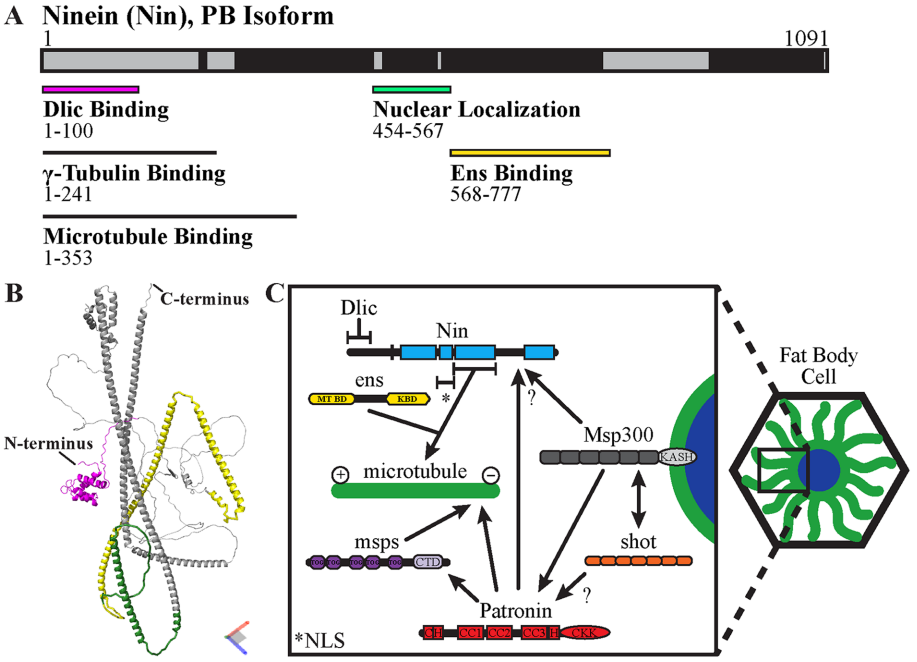

FIGURE 8: Summary of Nin domains and model depicting its cooperative role with ensconsin at the MTOC. (A) Summary of Nin domains mapped from this work that includes the Dlic and ens binding domains and the nuclear localization domain. (B) Location of Nin domains on the three-dimensional structure of Nin-PB predicted by AlphaFold (Jumper *et al.*, 2021; Varadi *et al.*, 2022). Color coding matches that in (A). (C) Model for the possible roles of Nin and ens at the fat body perinuclear MTOC, building on the model proposed recently (Zheng *et al.*, 2020). KASH = Klarsicht, ANC-1, Syne Homology domain. CTD = C-terminal domain. CKK = CAMSAP1, KIAA1078, KIAA1543 domain. MT BD = MT binding domain. KBD = Kinesin binding domain.

was inserted into pBID-UASC-GRM (RRID:Addgene_35203, [Wang *et al.*, 2012]), creating a C-terminal TagRFP-Myc-tagged Nin construct (pBID-UASC-Nin-GRM). A version of pBID-UASC-Nin-GRM was also generated to be RNAi resistant to the $Nin^{HMS23837}$ RNAi line (RRID:BDSC_62414). The primers used to create this plasmid introduced silent mutations (CAAGAGATTTCAAGTCTCCAG, mutations underlined) in the RNAi recognition motif (CAGGAAATCAGTTCACTGCAA). Either of these plasmids was used as a template for the construction of Nin constructs shown in Figure 1. PCR fragments were inserted into EcoR1- and Bsu36I-digested pBID-UASC-GRM plasmid using NEBuilder HiFi DNA Assembly (New England BioLabs, Catalogue #E5520S). Primers were designed using SnapGene and purchased from Integrated DNA Technologies. Primers and sequences are shown below. Constructs were verified by sequencing and transgenes were then inserted at VK40(3R) attP docking site by ΦC31 integration by GenetiVision, and screened in our lab. Transgenic lines were selected by expression of mini-white and confirmed by Western blotting and IF staining.

Primer name	Sequence	Length
1.FWD	CACCATGGAGGTATCCGCCGAT	22-mer
2.FWD	GACCCAGCTTTCTTGTACAAAGTGGTTGAT	30-mer
3.FWD	CTTTGAATCACAAGACGCATACCAAACGATGGAGGTATCCGCCGATCCGTAC	52-mer
4.FWD	CTTTGAATCACAAGACGCATACCAAACGATGGAACTGGCCCAAACGTCGAGCAGCATT	58-mer
5.FWD	CGCAAGTGCACCGAAGGAGAG	21-mer
6.FWD	CTTTGAATCACAAGACGCATACCAAACGATGCGCAAGTGCACCGAAGGA	49-mer
7.FWD	CAAGAGATTTCAAGTCTCCAGTCAGAGATCGAGGATTTGCGACAG	45-mer
8.FWD	CTTTGAATCACAAGACGCATACCAAACGATGGATTCGCCGAGCAAAACACAT	52-mer
9.FWD	CTTTGAATCACAAGACGCATACCAAACGATGGGAAAAAGTCCAGCCAGCTCA	52-mer
1.REV	AGGCATGCCAGGCAGTCCA	19-mer
2.REV	GACTCTCTCCCATGTGAAGCCCTC	24-mer
3.REV	ATCAACCACTTTGTACAAGAAAGCTGGGTCGTATGTGTTGTTTAGCGGCTCATC	54-mer
4.REV	ATCAACCACTTTGTACAAGAAAGCTGGGTCGGTGTCCAGTGATTCCACG	49-mer
5.REV	ATCAACCACTTTGTACAAGAAAGCTGGGTCCACGGCAAGCAAAGCCA	47-mer
6.REV	ATCAACCACTTTGTACAAGAAAGCTGGGTCGAGCTTAATGTTCTGTTCGAGAAG	54-mer
7.REV	ATCAACCACTTTGTACAAGAAAGCTGGGTCGGTGCACTTGCGCTGTTT	48-mer
8.REV	ATCGCTCTGCTCTCCTTCGGTGCACTTGCGCTTAATGTTCTGTTCGAGAAG	51-mer
9.REV	CTGGAGACTTGAAATCTCTTGAGCCTTCTCCTCGAGCATTTGAAT	45-mer
10.REV	ATCAACCACTTTGTACAAGAAAGCTGGGTCCAGTGCCGACGGACTGCT	48-mer

Fly stocks

Flies were maintained on standard food. Crosses were conducted at 29°C unless otherwise stated. For crosses involving tub-GAL80^{ts-7}, crosses were started at 25° and then moved to 29° on the third day. *w*^{1118} was used as wild-type.

Identifiers and sources for the fly strains used in this study can be found below. Bloomington *Drosophila* Stock Center = BDSC, Vienna *Drosophila* Resource Center = VDRC.

Mutant, RNAi, transgenic, or driver line used	Source
w[1118]	RRID:BDSC_3605
Nin[1]	(Zheng *et al.*, 2016)
αTub84B[JF01373]	RRID:BDSC_31389
Dhc64C[GL00543]	RRID:BDSC_36583
Dlic[GD9681]	RRID:BDSC_41686
ens[HMS00933]	RRID:BDSC_40825
klar[HMS01612]	RRID:BDSC_36721
klar[GD9271]	VDRC_32836
Luc[JF01355]	RRID:BDSC_31603
Msp300[KK112156]	VDRC_107183
msps[HMS01906]	RRID:BDSC_38990
Patronin[GD11946]	VDRC_27654
UAS-DCTN2-p50 (Dynamitin)	RRID:BDSC_8784
UAS-HA-Dhc	(Silvanovich *et al.*, 2003)
UAS-Dlic-GFP	(Zheng *et al.*, 2008)
UAS-ens-GFP	(Rosen *et al.*, 2019)
UAS-GFP	RRID:BDSC_5430
UAS-mCherry	RRID:BDSC_35787
UAS-Eos-Nin (III)	(Rosen *et al.*, 2019)
UAS-Nin-GFP	(Zheng *et al.*, 2016)
UAS-Nin-6 × Myc	(Zheng *et al.*, 2016)
UAS-CFP-spastin	(Du *et al.*, 2010)
Mef2-GAL4	RRID:BDSC_27390
SPARC-GAL4	RRID:BDSC_77473
SPARC-GAL4, GFP-Rab5	(Zheng *et al.*, 2020)
tub-GAL4[LL7]	RRID:BDSC_5138

The following lines were generated for this study:

Line
y[1], w[*];; UAS-Nin[1-1091]-TagRFP-Myc
y[1], w[*];; UAS-Nin[1-100]-TagRFP-Myc
y[1], w[*];; UAS-Nin[1-242]-TagRFP-Myc
y[1], w[*];; UAS-Nin[1-353]-TagRFP-Myc
y[1], w[*];; UAS-Nin[1-451]-TagRFP-Myc
y[1], w[*];; UAS-Nin[Δ451-567]-TagRFP-Myc
y[1], w[*];; UAS-Nin[1-571]-TagRFP-Myc
y[1], w[*];; UAS-Nin[454-571]-TagRFP-Myc
y[1], w[*];; UAS-Nin[454-1091]-TagRFP-Myc
y[1], w[*];; UAS-Nin[568-1091]-TagRFP-Myc
y[1], w[*];; UAS-Nin[550-924]-TagRFP-Myc
y[1], w[*];; UAS-Nin[778-1091]-TagRFP-Myc
w[*]; Nin[1]; SPARC-GAL4/TM6B, Hu[1], Tb[1]
w[*]; Nin[1]; UAS-Nin[1-1091]-TagRFP-Myc
w[*]; Nin[1]; UAS-Nin[1-100]-TagRFP-Myc
w[*]; Nin[1]; UAS-Nin[1-242]-TagRFP-Myc
w[*]; Nin[1]; UAS-Nin[1-353]-TagRFP-Myc
w[*]; Nin[1]; UAS-Nin[1-451]-TagRFP-Myc
w[*]; Nin[1]; UAS-Nin[Δ451-567]-TagRFP-Myc
w[*]; Nin[1]; UAS-Nin[1-571]-TagRFP-Myc
w[*]; Nin[1]; UAS-Nin[454-571]-TagRFP-Myc
w[*]; Nin[1]; UAS-Nin[454-1091]-TagRFP-Myc
w[*]; Nin[1]; UAS-Nin[568-1091]-TagRFP-Myc
Nin[1]; SPARC-GAL4, mCherry.nls[3]/TM6B, Hu[1], Tb[1]
w[*]; SPARC-GAL4, UAS-ens-GFP/TM6B, Hu[1], Tb[1]
SPARC-GAL4, UAS-Dlic-GFP/TM6B, Hu[1], Tb[1]
w[*]; UAS-Nin-GFP; tub-GAL4[LL7], tub-GAL80[ts-7]/TM6B, Hu[1], Tb[1]
αTub84B[JF01373], UAS-Nin[550-924]-TagRFP-Myc (II)
w[*];; SPARC-GAL4, UAS-Nin[1-1091]-TagRFP-Myc
w[*];; SPARC-GAL4, UAS-Nin[1-100]-TagRFP-Myc
w[*];; SPARC-GAL4, UAS-Nin[1-242]-TagRFP-Myc
w[*];; SPARC-GAL4, UAS-Nin[1-353]-TagRFP-Myc
w[*];; SPARC-GAL4, UAS-Nin[1-451]-TagRFP-Myc
w[*];; SPARC-GAL4, UAS-Nin[454-571]-TagRFP-Myc
w[*];; SPARC-GAL4, UAS-Nin[1-571]-TagRFP-Myc
w[*];; SPARC-GAL4, UAS-Nin[Δ451-567]-TagRFP-Myc
w[*];; SPARC-GAL4, UAS-Nin[568-1091]-TagRFP-Myc
w[*];; SPARC-GAL4, UAS-Nin[550-924]-TagRFP-Myc
w[*];; SPARC-GAL4, UAS-Nin[778-1091]-TagRFP-Myc
w[*];; SPARC-GAL4, UAS-Nin[454-1091]-TagRFP-Myc

Survey of Nin lethality

GAL4 driver virgin females were crossed to the indicated transgenes. UAS-mCherry and UAS-GFP/TM6B were used as controls. Progeny were screened for viability (i.e., eclosion from pupal case). Pupal lethality was also assessed and quantified. Crosses were repeated three times, and the results were averaged. RStudio "Ghost Orchid" Release (8b9ced18, 2021-11-08) 2021.09.1 Build 372 was used to graph the results compiled in a separate spreadsheet. The following code was used:

library("ggplot2")

Nin$Tag ← factor(Nin$Tag, levels = c("Nin-TagRFP-Myc", "Nin-GFP", "Eos-Nin", "mCherry", "GFP"))

Nin$GAL4 ← factor(Nin$GAL4, levels = c("tub-GAL4", "SPARC-GAL4", "GAL4-Mef2"))

```
ggplot(Nin,
  aes(x = Tag,
    y = Percent,
    fill = Key)) +
  geom_bar(stat = "identity",
      #color = "black",
      position = "stack") +
  scale_fill_grey(start = 0.8, end = 0.1) + theme_classic() +
  facet_grid(~ GAL4) +
  #labs(title = "Nin OE Lethality") +
  theme(axis.text.x = element_text(angle = 45, hjust = 1))
```

NLS database search

The sequences of Nin PB from amino acids 1–100 and 454–567 were separately analyzed with the following programs to check for nuclear localization sequences: NLStradamus (Nguyen Ba *et al.*, 2009) and NLS Predictor (NovoPro). Default settings were used for each program.

Immunostaining and imaging

Fat bodies were dissected from two wandering third instar larvae in 1X DPBS (Life Technologies, Ref#14080-055) and mounted on poly-Lysine-treated slides (Kao and Megraw, 2004; VWR, Catalogue#89085-339) in 12 µL of 4% paraformaldehyde (PFA, Spectrum, Catalogue#P1010). Two to four slides were prepared for each condition. After ~8 min in PFA, a siliconized 22 × 22 coverslip (VWR, Catalogue#48366-227) was applied, and the tissues were allowed to flatten for ~1 min before the slide was snap frozen in liquid nitrogen. Once frozen, the slide was removed from the liquid nitrogen, and the coverslip was quickly pried off using a razor blade. The slide was then immediately placed into a Coplin jar filled with phosphate-buffered saline (PBS), pH 7.3 (137 mM NaCl (OmniPur, Catalogue#7760), 2.7 mM KCl (OmniPur, Catalogue#7300), 8 mM Na_2HPO_4 (VWR, Catalogue#0404-500G), 1.4 mM KH_2PO_4 (Millipore, Catalogue#529568-250GM) before application of primary antibodies.

Once all samples had been processed, slides were dried, and a hydrophobic ring was drawn around the tissue sample using a Liquid Blocker Super PAP Pen (Electron Microscopy Sciences, Catalogue#71312). The sample was incubated overnight at 4°C with a blocking solution (PBS, 0.5% bovine serum albumin [Boehringer Mannheim Corp., Catalogue#100-021], 0.1% saponin [Sigma, Catalogue#S-2149]) in a dark humid chamber. The next day, slides were incubated with primary antibody either overnight at 4°C or for 4–6 h at room temperature. Following incubation with primary antibodies, samples were washed 3 × 10 min with PBS. Samples were then incubated with secondary antibodies for 1.25 h at room temperature. After secondary antibody incubation, samples were washed 3 × 5 min with PBS and then mounted in 15 µL of mounting media (80% Glycerol (Alfa Aesar, Catalogue#36646); 0.1 M Tris•HCl (Calbiochem, Catalogue#648311), pH 8.8; 0.05% p-phenylenediamine [Sigma Aldrich, Catalogue#P-1519]). Slides were imaged and analyzed on a Nikon A1R or AX confocal microscope with an Apo TIRF 60X/1.49 oil objective using NIS-Elements version 4.6 or 5.42 software. At least six larvae were imaged for each experiment, and the experiment was repeated at least three times.

Antibodies and stains

The following antibodies were used in this work: rat anti-α-tubulin (YL1/2; 1:1000 for immunofluorescence (IF); 1:3333 for immunoblotting (WB); Invitrogen, RRID:AB_2210201), mouse anti-Dlic monoclonal (P5F5; 1:5000 IF; gift from Tom Hays [Mische *et al.*, 2008]), mouse anti-Dic (MAB1618; 1:1000 WB; EMD Millipore, RRID:AB_1674698), rabbit anti-ensconsin (1:20 IF; 1:1000 WB; gift from Vladimir Gelfand, [Barlan *et al.*, 2013]), rabbit anti-HA tag (C29F4; 1:1000 IF; Cell Signaling Technology, Catalogue#3724, RRID:AB_1549585), chicken anti-GFP (1:5000 WB; Aves Labs, RRID:AB_2307313), rabbit anti-GFP (1:10000 WB; Invitrogen, RRID:AB_221570), mouse anti-LamC (LC28.26; 1:100 IF; DSHB deposited by P. A. Fisher, RRID:AB_528339, [Riemer *et al.*, 1995]), mouse anti-Myc tag (9B11; 1:5000 WB; Cell Signaling Technology, RRID:AB_331783), and guinea pig anti-Nin (1:1000 WB; gift from Eric Lécuyer). The following stains were used for IF staining: DAPI (DNA; 1 µg/mL; Sigma), Phalloidin-iFluor 488 (F-actin; 1:1000; AAT Bioquest, Catalogue#23115), Phalloidin-iFluor 568 Conjugate (F-actin; 1:1000; Invitrogen). Nin transgenes, ens-GFP, and Dlic-GFP did not require additional staining.

Quantification and analysis

To visualize a fluorescence intensity profile, images were opened in NIS-Elements AR 4.6 software > Measure > Intensity Profile. A single *z*-slice near the center of the stack was selected for measurement, and a ~30 µm line was drawn bisecting the nucleus. The fluorescence intensity profile was calculated automatically by the software.

Nuclear positioning was quantified using NIS-Elements AR 4.6 software, as previously described (Zheng *et al.*, 2020). The distance between the centroid of the autothresholded nuclear signal (DAPI staining) and the centroid of the auto- or manually thresholded cell boundary (Phalloidin staining) was measured for each cell. Over 100 cells were measured across at least three slides (experiments). Outliers (as defined by Tukey's fences) were removed from the data set.

Fiji (Fiji is just ImageJ, ImageJ2 version 2.14.0/1.54f build c89e8500e4) was used to quantify nuclear circularity, MT density, and Nin localization at the nuclear surface. Six larvae across three slides (experiments) were used to measure around 100 cells for each experimental condition. The average background signal for five nonperinuclear regions in each image was subtracted from the measurements. Results were analyzed using Student's *t*-test on GraphPad Prism 10 version 10.2.0 (355) analysis software.

For nuclear circularity, LamC signal was thresholded with smoothing, the image was converted to binary, and ROIs were created for each in-focus nucleus. Then, ROIs were measured with the circularity tool selected. Scores range from 0–1 with 1 being a true circle.

For MT density measurements, LamC or DAPI signal was thresholded with smoothing, the image was converted to binary, and ROIs were created for each in-focus nucleus. The ROIs were then dilated using the default settings to encompass the MT signal around the nucleus. Finally, ROIs were measured with the area and mean grey values tools selected to get an integrated intensity of the MT signal with this formula:

$$\text{Integrated Intensity} = \text{Area of ROI} \times (\text{Mean Intensity} - \text{Background Intensity})$$

For Nin localization measurements, a nuclear ROI was created, and the nuclear circularity measurements were measured with area and mean grey value tools selected to get the integrated intensity of Nin signal within the nucleus. Then, a dilated ROI was created for the MT intensity measurements and measured to get the integrated intensity of the Nin signal within and surrounding the nucleus. Nuclear integrated intensity was subtracted from dilated integrated intensity to get the integrated intensity outside the nucleus. The ratio of integrated intensity outside the nucleus compared with the total integrated intensity of the dilated ROI gave the percentage of

Nin that localized to the nuclear surface. Three larvae were analyzed and at least 10 cells were measured for each.

GFP-Trap magnetic beads

pBiex-1 GFPNanobody_SNAP plasmid (RRID:Addgene_82711) was expressed in *E. coli* strain BL21(DE3)pLysE and then purified by Ni^{2+}-immobilized metal affinity chromatography. A 1-cm diameter column was packed with 1.5 mL packed bed volume of Chelating Sepharose Fast Flow (Amersham Biosciences, Catalogue#17-0575-01). The column was washed with water before being charged with 5 mL of 10% $NiSO_4$ (Millipore Sigma, Catalogue#227676) and washed again with water, followed by a five-volume wash of Solution A (20 mM Tris, pH 8.0; 100 mM NaCl). The *E. coli* lysate was mixed with Ni^{2+}-charged sepharose and rocked at 4°C in the column for 15 min for binding. The lysate was then eluted from the column followed by a 10-volume Solution A wash and five to 10 volume wash of Solution B (20 mM Tris, pH 8.0; 100 mM NaCl; 15 mM Imidazole (Millipore Sigma, Catalogue#IX0005). Finally, column flow was stopped, and 2.5 mL of Solution C (20 mM Tris, pH 8.0; 100 mM NaCl; 300 mM Imidazole) was added. The column was then incubated at 4°C for 10 min before collecting the eluent. The purified GFPNanobody was dialyzed against PBS before coupling to NHS Mag Sepharose (Millipore Sigma, Catalogue#GE28-9440-09) following the product protocol.

coimmunoprecipitation

Twenty to forty larvae were collected, washed in water, dried on a paper towel, and then frozen at –80°C until all samples and controls had identical numbers of larvae. Using a micro pestle (VWR International Pestle, Catalogue#47747-366) and mechanical tissue homogenizer (VWR International Pellet Mixer, Ref#47747-370), larvae were homogenized in 500 µL of Lysis Buffer (10 mM Tris•HCl, pH 7.5; 150 mM NaCl (OmniPur, Catalogue#7760); 0.5 mM EDTA (OmniPur, Catalogue#4005); 0.5% Nonidet P40 Substitute (VWR, Catalogue#E109-100ML)) containing protease inhibitors (1 mM 1,10-phenanthroline monohydrate (Sigma-Aldrich, Catalogue#P9375-5G); 0.5 mM PMSF (Sigma, Catalogue#EM-7110); 1 mM benzamidine hydrochloride hydrate (Sigma-Aldrich, Catalogue#B6506-5G); 1X protease inhibitor cocktail (Sigma-Aldrich, Catalogue#P8340-1ML) and 0.4 mM nocodazole (Sigma, Catalogue#M1404-2MG). The lysates were incubated on ice for 30 min with light vortexing every 10 min. Then, lysates were centrifuged at 15,000×*g* for 6–7 min at 4°C and the cleared lysate was added to a precooled tube containing 300 µL of Dilution Buffer (10 mM Tris•HCl, pH 7.5; 150 mM NaCl; 0.5 mM EDTA) with protease inhibitors. This diluted lysate was then incubated with equilibrated GFP-Trap Magnetic beads (Chromotek, Catalogue#gtmak, RRID:AB_2631358) or beads made in-house (see above) for 45 min-1 h at 4°C with agitation. Following incubation, beads were washed 3 × 15 min with Dilution Buffer with protease inhibitors before being resuspended in 2X SDS–PAGE Loading Buffer (100 mM Tris•HCl, pH 6.8; 4% sodium dodecyl sulfate (J.T. Baker, Catalogue#4095-02); 0.02% Bromophenol Blue (FisherBiotech, Catalogue#BP115-25); 20% Glycerol; 5% BME (OmniPur, Catalogue#6010) for immediate analysis via Western blotting. For co-IP Western blots, input and unbound fractions represent ~1% of the total lysate and IP fractions represent 45–50% of the total immunoprecipitate.

To assess Nin multimerization, UAS-Nin-GFP; tub-GAL4[LL7], tub-GAL80[ts-7]/TM6B flies were crossed to UAS-Nin[1-1091]-TagRFP-Myc flies. To circumvent the lethality that arises with high levels of Nin overexpression, crosses were incubated at room temperature for 3 d and then shifted to 29° to derepress GAL80.

To map the Dlic interaction domain, 100 larvae were collected and processed as above in 1250 µL of Lysis Buffer.

co-IP experiments were repeated at least three times.

Western blotting and analysis

To verify expression from the Nin transgenes generated for this study, SPARC-GAL4 was used to drive expression of the transgenes in the fat body. Two larvae were collected, washed, and lysed using a micro pestle and mechanical tissue homogenizer in 40 µl of 2 × SDS–PAGE Loading Buffer. After incubating at 95°C for 5 min, larval lysates were quickly spun down, and 6 µl was loaded for SDS–PAGE gel electrophoresis on an 8% SDS–PAGE gel. The gel was transferred using a wet high-intensity field transfer for 1 h onto nitrocellulose membrane. The membrane was then blocked with 5% nonfat milk (Publix Instant Nonfat Dry Milk) in Tris-buffered saline (TBS; 0.5 M Tris•HCl, pH 7.5; 1.2 M NaCl) for 1 h at room temperature or overnight at 4°C with rocking. This was followed by a brief wash in TBST (Tris-buffered saline with 0.1% Tween 20 [Fisher Bioreagents, Catalogue#BP337-100]) to rinse out the milk.The membrane was then probed with primary antibodies diluted in TBST for 1.25 h at room temperature or overnight at 4°C with rocking. After washing with TBST 3 × 10 min, the membrane was incubated with secondary antibodies conjugated with IRDye-800CW or IRDye-680LT (1:20,000, LI-COR) for 1.25 h at room temperature with rocking. Blots were scanned on an Odyssey CLx-2666 Infrared Imager (LI-COR Biosciences) using Image Studio v 5.2.5 software (LI-COR).

To measure the expression of various Nin transgenes in the fat body, fat bodies were dissected from three wandering third instar larvae. Genital discs remained, but all other tissues and glands were removed. Fat bodies were then homogenized by pipetting in 20 µL of 2 × SDS–PAGE Loading Buffer and analyzed by Western blotting as above on a 10% SDS–PAGE gel. Blots were scanned on an Odyssey CLx-2666 Infrared Imager (LI-COR Biosciences) using Image Studio v 5.2.5 software (LI-COR). The normalized Nin signal was calculated using the Revert 700 Total Protein Stain Strategy (LI-COR, Catalogue#926-11011) published in the Normalization Handbook (rev. September 2019). Values shown are an average of three experiments normalized to wild-type control.

ACKNOWLEDGMENTS

We thank Eric Lécuyer for antibodies to Nin, Vladimir Gelfand for antibodies to ensconsin, and all the contributors to the Developmental Studies Hybridoma Bank (DSHB) for providing antibodies used in this study. DSHB was created by the NICHD of the National Institutes of Health and is maintained at The University of Iowa, Department of Biology, Iowa City, IA 52242. We thank Jerome Irianto for his help and training with Fiji. We thank Michael Welte for sharing his expertise on LINC complex proteins and functions, discussing the project during its infancy with us, and providing a critical reading of the manuscript. We thank Mary Baylies for UAS-Eos-Nin transgenic stocks, Tom Hays for UAS-HA-Dhc and an antibody to Dlic, Yuh-Nung Jan for UAS-Dlic-GFP, and Melissa Rolls for UAS-CFP-spastin. Many thanks to Bloomington Drosophila Stock Center (NIH P40OD018537), Vienna Drosophila Resource Center (Dietzl *et al.*, 2007), and FlyBase (Öztürk-Çolak *et al.*, 2024) for curating indispensable tools and resources. Thank you to Batory Foods for their generous donation of fly food reagents to support this work. We are also grateful to the members of the Megraw Lab for their countless hours of helpful discussion.

This work was supported by a Legacy Fellowship to Marisa Tillery from Florida State University, National Institutes of Health grant R01GM139971 to Timothy Megraw, and National Natural Science

Foundation of China grant (32370731) and Shenzhen Science and Technology Program grant (JCYJ20230807091308018) to Yiming Zheng.

REFERENCES

Abal M, Piel M, Bouckson-Castaing V, Mogensen M, Sibarita JB, Bornens M (2002). Microtubule release from the centrosome in migrating cells. J Cell Biol 159, 731–737.

Barlan K, Lu W, Gelfand VI (2013). The Microtubule-Binding Protein Ensconsin Is an Essential Cofactor of Kinesin-1. Current biology: CB 23, 317–322.

Baumbach J, Novak ZA, Raff JW, Wainman A (2015). Dissecting the function and assembly of acentriolar microtubule organizing centers in Drosophila cells in vivo. PLoS Genet 11, e1005261.

Biedzinski S, Agsu G, Vianay B, Delord M, Blanchoin L, Larghero J, Faivre L, Théry M, Brunet S (2020). Microtubules control nuclear shape and gene expression during early stages of hematopoietic differentiation. EMBO j 39, e103957.

Bouckson-Castaing V, Moudjou M, Ferguson DJ, Mucklow S, Belkaid Y, Milon G, Crocker PR (1996). Molecular characterisation of ninein, a new coiled-coil protein of the centrosome. J Cell Sci 109, 179–190.

Bugnard E, Zaal KJ, Ralston E (2005). Reorganization of microtubule nucleation during muscle differentiation. Cell Motil Cytoskeleton 60, 1–13.

Casenghi M, Barr FA, Nigg EA (2005). Phosphorylation of Nlp by Plk1 negatively regulates its dynein-dynactin-dependent targeting to the centrosome. J Cell Sci 118, 5101–5108.

Casenghi M, Meraldi P, Weinhart U, Duncan PI, Korner R, Nigg EA (2003). Polo-like kinase 1 regulates Nlp, a centrosome protein involved in microtubule nucleation. Dev Cell 5, 113–125.

Celestino R, Henen MA, Gama JB, Carvalho C, McCabe M, Barbosa DJ, Born A, Nichols PJ, Carvalho AX, Gassmann R, Vogeli B (2019). A transient helix in the disordered region of dynein light intermediate chain links the motor to structurally diverse adaptors for cargo transport. PLoS Biol 17, e3000100.

Chen F, Wu J, Iwanski MK, Jurriens D, Sandron A, Pasolli M, Puma G, Kromhout JZ, Yang C, Nijenhuis W, *et al*. (2022). Self-assembly of pericentriolar material in interphase cells lacking centrioles. eLife 11, e77892.

Cheng TS, Chang LK, Howng SL, Lu PJ, Lee CI, Hong YR (2006). SUMO-1 modification of centrosomal protein hNinein promotes hNinein nuclear localization. Life Sci 78, 1114–1120.

Dammermann A, Merdes A (2002). Assembly of centrosomal proteins and microtubule organization depends on PCM-1. J Cell Biol 159, 255–266.

Dauber A, Lafranchi SH, Maliga Z, Lui JC, Moon JE, McDeed C, Henke K, Zonana J, Kingman GA, Pers TH, *et al*. (2012). Novel microcephalic primordial dwarfism disorder associated with variants in the centrosomal protein ninein. J Clin Endocrinol Metab 97, E2140–2151.

Davidson PM, Lammerding J (2014). Broken nuclei–lamins, nuclear mechanics, and disease. Trends Cell Biol 24, 247–256.

Delgehyr N, Sillibourne J, Bornens M (2005). Microtubule nucleation and anchoring at the centrosome are independent processes linked by ninein function. J Cell Sci 118, 1565–1575.

Dietzl G, Chen D, Schnorrer F, Su KC, Barinova Y, Fellner M, Gasser B, Kinsey K, Oppel S, Scheiblauer S, *et al*. (2007). A genome-wide transgenic RNAi library for conditional gene inactivation in Drosophila. Nature 448, 151–156.

Du F, Ozdowski EF, Kotowski IK, Marchuk DA, Sherwood NT (2010). Functional conservation of human Spastin in a Drosophila model of autosomal dominant-hereditary spastic paraplegia. Hum Mol Genet 19, 1883–1896.

Dyachuk V, Bierkamp C, Merdes A (2016). Non-centrosomal Microtubule Organization in Differentiated Cells. In: The Microtubule Cytoskeleton: Organisation, Function and Role in Disease, ed. J. Lüders, Vienna: Springer Vienna, 27–41.

Emre D, Terracol R, Poncet A, Rahmani Z, Karess RE (2011). A mitotic role for Mad1 beyond the spindle checkpoint. J Cell Sci 124, 1664–1671.

Gilbert T, Gorlt C, Barbier M, Duployer B, Plozza M, Dufrancais O, Martet LE, Dalbard E, Segot L, Tenailleau C, *et al*. (2024). Loss of ninein interferes with osteoclast formation and causes premature ossification. Elife 13, e93457.

Goldspink DA, Rookyard C, Tyrrell BJ, Gadsby J, Perkins J, Lund EK, Galjart N, Thomas P, Wileman T, Mogensen MM (2017). Ninein is essential for apico-basal microtubule formation and CLIP-170 facilitates its redeployment to non-centrosomal microtubule organizing centres. Open Biol 7, 160274.

He L, van Beem L, Snel B, Hoogenraad CC, Harterink M (2022). PTRN-1 (CAMSAP) and NOCA-2 (NINEIN) are required for microtubule polarity in Caenorhabditis elegans dendrites. PLoS Biol 20, e3001855.

Heffler J, Shah PP, Robison P, Phyo S, Veliz K, Uchida K, Bogush A, Rhoades J, Jain R, Prosser BL (2020). A Balance Between Intermediate Filaments and Microtubules Maintains Nuclear Architecture in the Cardiomyocyte. Circ Res 126, e10–e26.

Inaba M, Buszczak M, Yamashita YM (2015). Nanotubes mediate niche–stem-cell signalling in the Drosophila testis. Nature 523, 329–332.

Jumper J, Evans R, Pritzel A, Green T, Figurnov M, Ronneberger O, Tunyasuvunakool K, Bates R, Zidek A, Potapenko A, *et al*. (2021). Highly accurate protein structure prediction with AlphaFold. Nature 596, 583–589.

Kao LR, Megraw TL (2004). RNAi in cultured Drosophila cells. Methods Mol Biol 247, 443–457.

Keminer O, Peters R (1999). Permeability of single nuclear pores. Biophys J 77, 217–228.

Kowanda M, Bergalet J, Wieczorek M, Brouhard G, Lecuyer E, Lasko P (2016). Loss of function of the Drosophila Ninein-related centrosomal protein Bsg25D causes mitotic defects and impairs embryonic development. Biol Open 5, 1040–1051.

Lechler T, Fuchs E (2007). Desmoplakin: an unexpected regulator of microtubule organization in the epidermis. J Cell Biol 176, 147–154.

Lecland N, Hsu CY, Chemin C, Merdes A, Bierkamp C (2019). Epidermal development requires ninein for spindle orientation and cortical microtubule organization. Life Sci Alliance 2, e201900373.

Lee IG, Cason SE, Alqassim SS, Holzbaur ELF, Dominguez R (2020). A tunable LIC1-adaptor interaction modulates dynein activity in a cargo-specific manner. Nat Commun 11, 5695.

Lin CC, Cheng TS, Hsu CM, Wu CH, Chang LS, Shen ZS, Yeh HM, Chang LK, Howng SL, Hong YR (2006). Characterization and functional aspects of human ninein isoforms that regulated by centrosomal targeting signals and evidence for docking sites to direct gamma-tubulin. Cell cycle 5, 2517–2527.

Matsumoto T, Schiller P, Dieterich LC, Bahram F, Iribe Y, Hellman U, Wikner C, Chan G, Claesson-Welsh L, Dimberg A (2008). Ninein is expressed in the cytoplasm of angiogenic tip-cells and regulates tubular morphogenesis of endothelial cells. Arterioscler Thromb Vasc Biol 28, 2123–2130.

Mische S, He Y, Ma L, Li M, Serr M, Hays TS (2008). Dynein light intermediate chain: an essential subunit that contributes to spindle checkpoint inactivation. Mol Biol Cell 19, 4918–4929.

Mogensen MM, Malik A, Piel M, Bouckson-Castaing V, Bornens M (2000). Microtubule minus-end anchorage at centrosomal and non-centrosomal sites: The role of ninein. J Cell Sci 113, 3013–3023.

Moss DK, Bellett G, Carter JM, Liovic M, Keynton J, Prescott AR, Lane EB, Mogensen MM (2007). Ninein is released from the centrosome and moves bi-directionally along microtubules. J Cell Sci 120, 3064–3074.

Muroyama A, Lechler T (2017). Microtubule organization, dynamics and functions in differentiated cells. Development 144, 3012–3021.

Nguyen Ba AN, Pogoutse A, Provart N, Moses AM (2009). NLStradamus: a simple Hidden Markov Model for nuclear localization signal prediction. BMC Bioinformatics 10, 202.

Omer S, Li J, Yang CX, Harrison RE (2024). Ninein promotes F-actin cup formation and inward phagosome movement during phagocytosis in macrophages. Mol Biol Cell 35, ar26.

Ou YY, Mack GJ, Zhang M, Rattner JB (2002). CEP110 and ninein are located in a specific domain of the centrosome associated with centrosome maturation. J Cell Sci 115, 1825–1835.

Öztürk-Çolak A, Marygold SJ, Antonazzo G, Attrill H, Goutte-Gattat D, Jenkins VK, Matthews BB, Millburn G, dos Santos G, Tabone CJ, Consortium F (2024). FlyBase: updates to the Drosophila genes and genomes database. Genetics 227, iyad211.

Pandey R, Heeger S, Lehner CF (2007). Rapid effects of acute anoxia on spindle kinetochore interactions activate the mitotic spindle checkpoint. J Cell Sci 120, 2807–2818.

Paz J, Luders J (2018). Microtubule-Organizing Centers: Towards a Minimal Parts List. Trends Cell Biol 28, 176–187.

Reck-Peterson SL, Redwine WB, Vale RD, Carter AP (2018). The cytoplasmic dynein transport machinery and its many cargoes. Nat Rev Mol Cell Biol 19, 382–398.

Redwine WB, DeSantis ME, Hollyer I, Htet ZM, Tran PT, Swanson SK, Florens L, Washburn MP, Reck-Peterson SL (2017). The human cytoplasmic dynein interactome reveals novel activators of motility. Elife 6, e28257.

Riemer D, Stuurman N, Berrios M, Hunter C, Fisher PA, Weber K (1995). Expression of Drosophila lamin C is developmentally regulated:

analogies with vertebrate A-type lamins. J Cell Sci 108(Pt 10), 3189–3198.
Rosen JN, Azevedo M, Soffar DB, Boyko VP, Brendel MB, Schulman VK, Baylies MK (2019). The Drosophila Ninein homologue Bsg25D cooperates with Ensconsin in myonuclear positioning. J Cell Biol 218, 524–540.
Royall LN, Machado D, Jessberger S, Denoth-Lippuner A (2023). Asymmetric inheritance of centrosomes maintains stem cell properties in human neural progenitor cells. Elife 12, e83157.
Sanchez AD, Feldman JL (2017). Microtubule-organizing centers: from the centrosome to non-centrosomal sites. Curr Opin Cell Biol 44, 93–101.
Shinohara H, Sakayori N, Takahashi M, Osumi N (2013). Ninein is essential for the maintenance of the cortical progenitor character by anchoring the centrosome to microtubules. Biol Open 2, 739–749.
Silvanovich A, Li MG, Serr M, Mische S, Hays TS (2003). The third P-loop domain in cytoplasmic dynein heavy chain is essential for dynein motor function and ATP-sensitive microtubule binding. Mol Biol Cell 14, 1355–1365.
Stevens DA, Beierschmitt C, Mahesula S, Corley MR, Salogiannis J, Tsu BV, Cao B, Ryan AP, Hakozawki H, Reck-Peterson SL, Daugherty MD (2022). Antiviral function and viral antagonism of the rapidly evolving dynein activating adaptor NINL. eLife 11, e81606.
Tillery MML, Blake-Hedges C, Zheng Y, Buchwalter RA, Megraw TL (2018). Centrosomal and Non-Centrosomal Microtubule-Organizing Centers (MTOCs) in Drosophila melanogaster. Cells 7, 121.
Timney BL, Raveh B, Mironska R, Trivedi JM, Kim SJ, Russel D, Wente SR, Sali A, Rout MP (2016). Simple rules for passive diffusion through the nuclear pore complex. J Cell Biol 215, 57–76.
van Wijk E, Kersten FF, Kartono A, Mans DA, Brandwijk K, Letteboer SJ, Peters TA, Märker T, Yan X, Cremers CW, *et al*. (2009). Usher syndrome and Leber congenital amaurosis are molecularly linked via a novel isoform of the centrosomal ninein-like protein. Hum Mol Genet 18, 51–64.
Varadi M, Anyango S, Deshpande M, Nair S, Natassia C, Yordanova G, Yuan D, Stroe O, Wood G, Laydon A, *et al*. (2022). AlphaFold Protein Structure Database: massively expanding the structural coverage of protein-sequence space with high-accuracy models. Nucleic Acids Res 50, D439–D444.
Vineethakumari C, Luders J (2022). Microtubule Anchoring: Attaching Dynamic Polymers to Cellular Structures. Front Cell Dev Biol 10, 867870.
Wainman A, Giansanti MG, Goldberg ML, Gatti M (2012). The Drosophila RZZ complex - roles in membrane trafficking and cytokinesis. J Cell Sci 125, 4014–4025.
Wang JW, Beck ES, McCabe BD (2012). A modular toolset for recombination transgenesis and neurogenetic analysis of Drosophila. PLoS One 7, e42102.
Wang R, Brattain MG (2007). The maximal size of protein to diffuse through the nuclear pore is larger than 60kDa. FEBS Lett 581, 3164–3170.
Wang S, Wu D, Quintin S, Green RA, Cheerambathur DK, Ochoa SD, Desai A, Oegema K (2015). NOCA-1 functions with gamma-tubulin and in parallel to Patronin to assemble non-centrosomal microtubule arrays in C. elegans. eLife 4, e08649.
Wang X, Tsai JW, Imai JH, Lian WN, Vallee RB, Shi SH (2009). Asymmetric centrosome inheritance maintains neural progenitors in the neocortex. Nature 461, 947–955.
Wu J, Akhmanova A (2017). Microtubule-Organizing Centers. Annu Rev Cell Dev Biol 33, 51–75.
Zhang X, Chen MH, Wu X, Kodani A, Fan J, Doan R, Ozawa M, Ma J, Yoshida N, Reiter JF, *et al*. (2016). Cell-Type-Specific Alternative Splicing Governs Cell Fate in the Developing Cerebral Cortex. Cell 166, 1147–1162 e1115.
Zheng Y, Buchwalter RA, Zheng C, Wight EM, Chen JV, Megraw TL (2020). A perinuclear microtubule-organizing centre controls nuclear positioning and basement membrane secretion. Nat Cell Biol 22, 297–309.
Zheng Y, Mennella V, Marks S, Wildonger J, Elnagdi E, Agard D, Megraw TL (2016). The Seckel syndrome and centrosomal protein Ninein localizes asymmetrically to stem cell centrosomes but is not required for normal development, behavior, or DNA damage response in Drosophila. Mol Biol Cell 27, 1740–1752.
Zheng Y, Wildonger J, Ye B, Zhang Y, Kita A, Younger SH, Zimmerman S, Jan LY, Jan YN. (2008). Dynein is required for polarized dendritic transport and uniform microtubule orientation in axons. Nat Cell Biol 10, 1172–1180.